Remotely-sensed image fusion based on generalized IHS transformation and MAP analysis

SHI Aiye, XU Lizhong, TANG Min

College of Computer and Information Engineering, *Hohai University*, *Jiangsu Nanjing* 210098, *China*

Abstract: This paper proposes a fusion method by combining generalized intensity-hue-saturation (GIHS) transformation and *maximum a posteriori* (MAP) analysis in order to improve the fusion quality of multispectral (MS) and panchromatic (Pan) images from a new type of remote sensing platforms. The intensity component of the MS images is first obtained by GIHS transformation. Then a new Pan image is acquired by combing the intensity component and Pan image using a steepest-descent optimization algorithm based on the MAP framework. Thus, the fused images are obtained by the GIHS method. Experiments are conducted using the IKONOS MS and Pan images, and Quickbird MS and Pan images. The proposed method is compared with the GIHS fusion method, the wavelet transform (WT) fusion method, and the combined WT-GIHS fusion method. The experimental results show that the proposed method can achieve better fusion result than exiting fusion methods.

Key words: remote sensing, image fusion, IHS transformation, wavelet transform, maximum a posteriori analysis

CLC number: TP751 **Document code:** A

Citation format: Shi A Y, Xu L Z and Tang M. 2010. Remotely-sensed image fusion based on generalized IHS transformation and MAP analysis. *Journal of Remote Sensing*. **14**(6): 1259—1272

1 INTRODUCTION

For a new type of high-spatial-resolution satellites, such as IKONOS satellite, it is desirable to choose an effective fusion method for the MS and Pan images from the satellite platforms, which can make the fused images not only hold the spatial detailed information of the Pan image but also keep the spectral information of the original MS images.

The common fusion methods for remotely sensed images mainly include generic component substitution methods (Choi, 2006; Tu *et al.,* 2004; Xu *et al.,* 2009) and multi-resolution analysis methods (González-Audícana *et al.,* 2004, 2008; Li *et al.,* 2009; Pohl & Van Genderen, 1998; Shah *et al.,* 2008; Tomas *et al.,* 2008; Zhou *et al.,* 1998).

Among the component substitution fusion methods, the IHS-based fusion methods are popular. Although the spatial enhancement of the IHS-fused MS images is high, the spectral distortion of these methods is considerable. In order to overcome the shortcoming of IHS-based fusion methods, Tu *et al*. (2004) proposed a generalized IHS (GIHS) fusion method based on linear IHS. In this study, the intensity component I is the average digital number (DN) values of red (R) band, green (G) band, blue (B) band and near Infrared (NIR) band. The main feature of this method is that inverse IHS transform is not needed, so the process of fusion includes only some addition and substraction operations among the MS image, Pan image and I component. Thus, the method decreases the computational cost. The spectral distortion of the method is still large, but some improvement.

In order to overcome the deficiency of the IHS fusion methods or the GIHS fusion methods, Choi (2006) improve the performance of the GIHS-based methods using the trade-off parameter in the fusion. The spectral and spatial detail quality of the method can be controlled by adjusting trade-off parameter. The disadvantage of the method is not to give how to choose the optimal trade-off parameter (Tomas *et al.,* 2008). Gonzalez- Audicana *et al*. (2004) proposed a fast remotely sensed fusion method using the GIHS transform based on spectral response function. The drawback of the method is that when constructing spectral response of sensor, the choice of parameter is estimated by priori knowledge. Furthermore, the method is only applied to the fusion of the IKONOS MS and Pan images.

The area of multiresolution fusion is quite mature, with many researchers attempting to solve this problem for remote sensing applications. The most common method is the WT-based fusion methods (Pohl *et al*., 1998; Zhou *et al*., 1998; Tomas *et al*., 2008). Since separable wavelets can capture only three limited directional information, namely horizontal, vertical and diagonal directions, WT is not optimal when used in analyzing linear/curve singularities in image processing. In order to overcome the defect, contourlet transform are introduced into the fusion of the remotely sensed images, and the

Received: 2010-01-15; **Accepted**: 2010-04-18

Foundation: National Natural Science Foundation of China (No.60774092, No.60872096 and No. 60901003), Specialized Research Fund for the Doctoral Program of Higher Education (No.20070294027).

First author biography: SHI Aiye(1969—), male, Lecturer. He received the Ph.D. degree from Hohai University, Jiangsu Nanjing, China, in 2009. He is focusing on the research of remotely sensed images processing. E-mail: ayshi.hhu@gmail.com

(C)1994-2021 China Academic Journal Electronic Publishing House. All rights reserved. http://www.cnki.net

fusion performance is improved (Song *et al.,* 2007). The disadvantage of the fusion method is its computation comp- lexity because of its multidirection of the transform (Shah *et al*., 2008).

Recently, fusion methods based on the IHS transformation and WT have merged (González-Audícana *et al*., 2004). The principle is described as follows. Firstly, a new intensity component is obtained by fusing the intensity component of the original MS images and Pan images by using WT. Then the inverse IHS transform is performed to obtain the fused images. The fusion quality of the methods is improved by combing the merits of wavelet transform and IHS transform. However, there are some limitations of the methods, such as how to choose the appropriate wavelet base, how to determine the decomposition level and how to adopt the fusion rule.

In order to improve the quality of the fused images, this paper proposes a fusion method based MAP on the basis of GIHS for new type high resolution remote sensing images. It is considered that MAP estimation can embed with priori knowledge and impose bounded constrains on the intensity component and panchromatic image to restrict the scope of solution. Thus, the final fused images can improve the quality of spatial detail and spectral information.

The structure of this paper is organized as follows. The principle of GIHS fusion method is briefly described in Section 2.1. The MAP based fusion method is introduced in Section 2.2. Then, the implementation steps of the proposed method are given in Section 2.3. The experiments on IKONOS imagery and Quickbird imagery are conducted in comparison with existing fusion methods in Section 3. A conclusion is drawn at the end.

2 THE PROPOSED METHOD

2.1 GIHS fusion method

For the fusion of IKONOS Pan and MS images, considering that the spectral range of the Pan image cover NIR, *R*, *G* and *B* bands of the MS images, Tu *et al.*(2004) introduced the NIR band into the computation of intensity of MS image, and adopted GIHS fusion method to overcome the spectral distortion.

Suppose, $X\in\{\text{NIR}, R, G, B\}$ and the fused image can be computed as

$$\boldsymbol{F}_X = \boldsymbol{M}_X^{\text{upsample}} + (\boldsymbol{P} - \boldsymbol{I}_{\text{g}}) \tag{1}$$

where $\boldsymbol{P}$ represents the DN values of the original Pan image and rep $\boldsymbol{M}_X$ resents the DN values of X band of the original MS images, $\boldsymbol{M}_X^{\text{upsample}}$ is the up-sampling images of X band of the original MS images (with a factor of 4), $\boldsymbol{I}_{\text{g}}$ represents the intensity component of the up-sampled MS images and is defined by

$$\boldsymbol{I}_{\text{g}}=\frac{1}{4}\sum_{X\in\{\text{NIR},R,G,B\}}\boldsymbol{M}_X^{\text{upsample}} \tag{2}$$

From Eq.(1), it can be seen that the NIR band of the MS images is included into the definition of the $\boldsymbol{I}_{\text{g}}$ component for the GIHS fusion method, although this reduces the spectral distortion to some extent, the spectral distortion problem still exists, and the fusion performance needs to be further improved.

In order to solve the above problem, this paper presents a fusion method using MAP statistical method to obtain a new high-resolution image $\boldsymbol{i}_{new}$, which replaces the Pan image $\boldsymbol{P}$ in Eq.(1), and Eq.(1) can be also rewritten as

$$\boldsymbol{F}_X = \boldsymbol{M}_X^{\text{upsample}} + \left(\boldsymbol{i}_{\text{new}} - \boldsymbol{I}_{\text{g}}\right) \tag{3}$$

where the high resolution image $\boldsymbol{i}_{new}$ is obtained by combining the intensity component of MS images and Pan image under the MAP framework. Thus the fused images can improve the spatial resolution while reserving the spectral information of the original MS images.

2.2 MAP estimation method

The proposed method first gives the MAP framework of high-resolution image $\boldsymbol{i}_{new}$, the intensity component of the original low-resolution MS images and Pan image based on the observation model. Then the estimation of $\boldsymbol{i}_{new}$ is obtained by gradient descent optimization algorithm. Here we mainly concentrate on the fusion of IKONOS MS and Pan images and the fusion of Quickbird MS and Pan images. Without generality, losing the proposed method is described by the fusion of IKONOS MS and Pan images.

2.2.1 Observation model

Suppose the ideal high resolution MS images be $\boldsymbol{z}$ with four bands: NIR, *R*, *G* and *B* bands. The DN values of the NIR, *R*, *G* and *B* bands are defined by z_{NIR}, z_R, z_G, z_B respectively. Suppose the noise of each band is independent identically distributed (i.i.d) Gaussian random noise, with zero mean and variance β_X^{-1} ($X\in\{\text{NIR}, R, G, B\}$). We have

$$p(\boldsymbol{n}_X) = \frac{1}{(2\pi)^{M/2}(1/\beta_X)^{M/2}}\times \exp\left\{-\frac{1}{2}\beta_X\sum(\boldsymbol{n}_X\odot\boldsymbol{n}_X)\right\} \tag{4}$$

where $\boldsymbol{n}_x$ represents the noise of *X* band, for $X\in\{\text{NIR}, R, G, B\}$

Then the degradation model of *X* band of the ideal MS image $\boldsymbol{z}$ can be expressed as

$$\boldsymbol{M}_X = \boldsymbol{W}\boldsymbol{z}_X + \boldsymbol{n}_X \tag{5}$$

where $\boldsymbol{W}$ represents PSF (point spread function) of remotely sensed imaging system, which is composed of the operation of blurring and undersampling, that is $\boldsymbol{W}=\boldsymbol{D}\boldsymbol{H}$, where $\boldsymbol{D}$ represents the undersampling operation with a factor of 4 along the rows and columns of the image and $\boldsymbol{H}$ is approximately represent as $\boldsymbol{H}=\frac{1}{16}\boldsymbol{I}_4$ (Mohamed & Mohammad, 2008), where $\boldsymbol{I}_4$ is a 4 by 4 matrix of ones.

From Eq.(5), we have

$$\frac{1}{4}\sum_{X\in\{\text{NIR},R,G,B\}}\boldsymbol{M}_X = \frac{1}{4}\boldsymbol{W}\sum_{X\in\{\text{NIR},R,G,B\}}\boldsymbol{z}_X + \frac{1}{4}\sum_{X\in\{\text{NIR},R,G,B\}}\boldsymbol{n}_X \tag{6}$$

which can also be rewritten as

$$\boldsymbol{I}_l = \boldsymbol{W}\boldsymbol{i}_{\text{new}} + \boldsymbol{n} \tag{7}$$

(C)1994-2021 China Academic Journal Electronic Publishing House. All rights reserved. http://www.cnki.net

where $\boldsymbol{I}_l = \frac{1}{4}\sum_{X\in\{\mathrm{NIR},R,G,B\}} \boldsymbol{M}_X$, $\boldsymbol{i}_{\mathrm{new}} = \frac{1}{4}\sum_{X\in\{\mathrm{NIR},R,G,B\}} \boldsymbol{z}_X$, $\boldsymbol{n} = \frac{1}{4}\sum_{X\in\{\mathrm{NIR},R,G,B\}} \boldsymbol{n}_X$ and $\boldsymbol{n}$ is a Gaussian random noise with zero mean and variance β^{-1} (which is relevant to $\beta_{\mathrm{NIR}}^{-1}$, β_R^{-1}, β_G^{-1}, β_B^{-1})

In addition, the Pan image P is formed as a linear combination of the ideal high-resolution MS images plus additive noise

$$\boldsymbol{P} = \sum_{X\in\{\mathrm{NIR},R,G,B\}} \lambda_X \boldsymbol{z}_X + \boldsymbol{v} \tag{8}$$

where **v** is the Gaussian random noise with 0 of mean value and γ^{-1} of variance, and γ_X ($X\in\{\mathrm{NIR}, R, G, B\}$) are known quantities weighting the contribution of each high resolution band we want to estimate to the high-resolution panchromatic image.

For IKONOS imagery, its spectral response curve can be depicted in Fig. 1, from IKONOS Relative Spectral Response of GeoEye Corporation (2008). From Fig. 1, it can be seen that each band of IKONOS MS images approximately covers the 1/4 width of the spectral range of the IKONOS Pan image. Therefore γ_X can be expressed as

$$\lambda_{\mathrm{NIR}} = \lambda_R = \lambda_G = \lambda_B = 1/4 \tag{9}$$

Thus Eq.(8) can be written as

$$\boldsymbol{P} = \boldsymbol{i}_{\mathrm{new}} + \boldsymbol{v} \tag{10}$$

2.2.2 MAP estimation

The MAP estimation is to find a high resolution estimation $\hat{\boldsymbol{i}}_{\mathrm{new}}$, which can be computed by

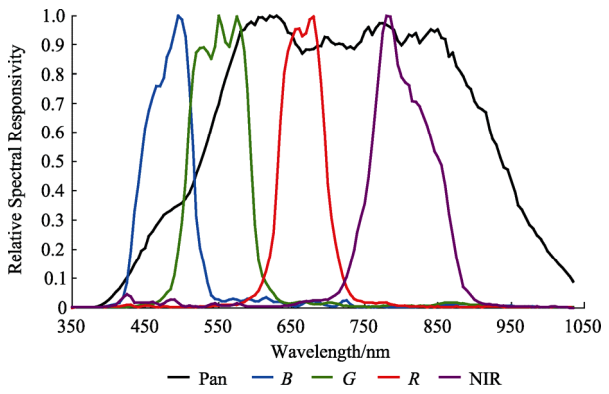

Fig. 1 IKONOS relative spectral response curve

$$\hat{\boldsymbol{i}}_{\mathrm{new}} = \arg\max_{\boldsymbol{i}_{\mathrm{new}}} \left[\Pr_{\boldsymbol{i}_{\mathrm{new}}\boldsymbol{I}_l,\boldsymbol{P}}(\boldsymbol{i}_{\mathrm{new}} \mid \boldsymbol{I}_l, \boldsymbol{P})\right] \tag{11}$$

With the Bayes rule, Eq.(11) can be represented as

$$\hat{\boldsymbol{i}}_{\mathrm{new}} = \arg\max_{\boldsymbol{i}_{\mathrm{new}}} \frac{\Pr_{\boldsymbol{I}_l,\boldsymbol{P}|\boldsymbol{i}_{\mathrm{new}}}(\boldsymbol{I}_l,\boldsymbol{P} \mid \boldsymbol{i}_{\mathrm{new}})\Pr(\boldsymbol{i}_{\mathrm{new}})}{\Pr(\boldsymbol{I}_l,\boldsymbol{P})} \tag{12}$$

Because the denominator of Eq.(12) is not a function of $\boldsymbol{i}_{\mathrm{new}}$, so Eq.(12) can be also expressed as:

$$\hat{\boldsymbol{i}}_{\mathrm{new}} = \arg\max_{\boldsymbol{i}_{\mathrm{new}}} \Pr_{\boldsymbol{I}_l,\boldsymbol{P}|\boldsymbol{i}_{\mathrm{new}}}(\boldsymbol{I}_l,\boldsymbol{P} \mid \boldsymbol{i}_{\mathrm{new}})\Pr(\boldsymbol{i}_{\mathrm{new}}) = \arg\max_{\boldsymbol{i}_{\mathrm{new}}} \Pr_{\boldsymbol{I}_l|\boldsymbol{i}_{\mathrm{new}}}(\boldsymbol{I}_l \mid \boldsymbol{i}_{\mathrm{new}})\Pr_{\boldsymbol{p}|\boldsymbol{i}_{\mathrm{new}}}(\boldsymbol{P} \mid \boldsymbol{i}_{\mathrm{new}})\Pr(\boldsymbol{i}_{\mathrm{new}}) \tag{13}$$

Assume the above probability density function $\Pr(\boldsymbol{i}_{\mathrm{new}})$ is a simultaneous auto-regression, i.e., $\Pr(\boldsymbol{i}_{\mathrm{new}}) \propto \exp\left\{-\frac{1}{2}\alpha\|\boldsymbol{C}\boldsymbol{i}_{\mathrm{new}}\|^2\right\}$, where C denotes the Gaussian kernel and α is the inverse of the inverse of the variance of the Gaussian distribution. According to Eq.(7) and Eq.(10), the MAP estimate of $\boldsymbol{i}_{\mathrm{new}}$ can be given as

$$\hat{\boldsymbol{i}}_{\mathrm{new}} = \arg\min_{\boldsymbol{i}_{\mathrm{new}}} L(\boldsymbol{i}_{\mathrm{new}}) = \arg\min_{\boldsymbol{i}_{\mathrm{new}}} \left(\frac{1}{2}\beta\|\boldsymbol{I}_l - \boldsymbol{W}\boldsymbol{i}_{\mathrm{new}}\|_2^2 + \frac{1}{2}\gamma\|\boldsymbol{P} - \boldsymbol{i}_{\mathrm{new}}\|_2^2 + \frac{1}{2}\alpha\|\boldsymbol{C}\boldsymbol{i}_{\mathrm{new}}\|_2^2\right) \tag{14}$$

The first term in Eq.(14) constrains the reconstructed image to be fidelity to intensity component of the original low-resolution MS images. The second term in Eq.(14) constrains the reconstructed image to be fidelity to the Pan image. The third term in Eq.(14) constrains the smoothness of the reconstructed image. By the appropriate choice of the parameters α, β, γ, the reconstructed image $\hat{\boldsymbol{i}}_{\mathrm{new}}$ can not only keep the spectral information of the original MS images, but also have the spatial detail information of the Pan image.

2.2.3 Gradient descent optimization algorithm

Taking into account the complexity of the optimization algorithm, we adopt simple gradient descent optimization algorithm to solve the high-resolution image $\boldsymbol{i}_{\mathrm{new}}$. The gradient of the cost function in Eq.(14) with respect to $\boldsymbol{i}_{\mathrm{new}}$ is given as

$$g(\boldsymbol{i}_{\mathrm{new}}) = \frac{\partial L(\boldsymbol{i}_{\mathrm{new}})}{\partial \boldsymbol{i}_{\mathrm{new}}} = \beta\boldsymbol{W}^{\mathrm{T}}(\boldsymbol{W}\boldsymbol{i}_{\mathrm{new}} - \boldsymbol{I}_l) + \gamma(\boldsymbol{i}_{\mathrm{new}} - \boldsymbol{P}) + \alpha\boldsymbol{C}^{\mathrm{T}}\boldsymbol{C}\boldsymbol{i}_{\mathrm{new}} \tag{15}$$

where the matrix W^{T} denotes the transpose of W, and C^{T} denotes the transpose of **C**.

The update of high-resolution estimate $\hat{\boldsymbol{i}}_{\mathrm{new}}$ is given as

$$\hat{\boldsymbol{i}}_{\mathrm{new}}^{k+1} = \hat{\boldsymbol{i}}_{\mathrm{new}}^{k} - \varepsilon^k g(\boldsymbol{i}_{\mathrm{new}})|_{\boldsymbol{i}_{\mathrm{new}}=\hat{\boldsymbol{i}}_{\mathrm{new}}^{k}} \tag{16}$$

where ε^k represents the step size at the *k*-th iteration. The choice of the parameter must be selected to be small enough to prevent divergence, and large enough to provide convergence at given iteration. The optimization iteration step is given by the minimization of

$$L\left(\hat{\boldsymbol{i}}_{\mathrm{new}}^{k+1}\right) = L\left(\hat{\boldsymbol{i}}_{\mathrm{new}}^{k} - \varepsilon^k g(\boldsymbol{i}_{\mathrm{new}})|_{\boldsymbol{i}_{\mathrm{new}}=\hat{\boldsymbol{i}}_{\mathrm{new}}^{k}}\right) \tag{17}$$

Differentiate Eq.(17) with respect to ε^k and set the result equal to zero, then have the step size as

$$\varepsilon^k = \frac{\beta\sum\left[\xi\odot\left(\boldsymbol{W}\hat{\boldsymbol{i}}_{\mathrm{new}}^{k} - \boldsymbol{I}_l\right)\right] + \alpha\sum\left[\psi\odot\boldsymbol{C}\hat{\boldsymbol{i}}_{\mathrm{new}}^{k}\right] + \gamma\sum\left[g\left(\hat{\boldsymbol{i}}_{\mathrm{new}}^{k}\right)\odot\left(\hat{\boldsymbol{i}}_{\mathrm{new}}^{k} - \boldsymbol{P}\right)\right]}{\beta\sum[\xi\odot\xi] + \alpha\sum[\psi\odot\psi] + \gamma\sum\left[g\left(\hat{\boldsymbol{i}}_{\mathrm{new}}^{k}\right)\odot g\left(\hat{\boldsymbol{i}}_{\mathrm{new}}^{k}\right)\right]} \tag{18}$$

where operator $\odot$ represents the element-by-element product of two matrix and ξ and ψ are defined as:

(C)1994-2021 China Academic Journal Electronic Publishing House. All rights reserved. http://www.cnki.net

$\xi = Wg\left(\hat{\boldsymbol{i}}_{new}^{k}\right)$, $\psi = \boldsymbol{C}g\left(\hat{\boldsymbol{i}}_{new}^{k}\right)$.

2.3 Steps of the proposed method

The implementation of the proposed method is described as follows:

Step 1 Compute the intensity component $\boldsymbol{I}_I$ of the original low resolution MS images based on GIHS.

Step 2 Begin at k=0 with the initial estimate $\hat{\boldsymbol{i}}_{\text{new}}^{0}$ being the intensity component of the bicubic interpolation of low resolution MS images and give the threshold q for terminating the iteration process.

Step 3 Compute the gradient $g(\boldsymbol{i}_{\text{new}})|_{\boldsymbol{i}_{\text{new}}=\hat{\boldsymbol{i}}_{\text{new}}^{k}}$ according to Eq.(15).

Step 4 Compute $\hat{\boldsymbol{i}}_{\text{new}}^{k+1}$ according to Eq.(16) and Eq.(18).

Step 5 If $\left\|\hat{\boldsymbol{i}}_{\text{new}}^{k+1}-\hat{\boldsymbol{i}}_{\text{new}}^{k}\right\| \Big/ \hat{\boldsymbol{i}}_{\text{new}}^{k} \leqslant q$ and the set number is reached, stop and go to step 7.

Step 6 Let k=k+1, go to step 3.

Step 7 Obtain the fused images by Eq.(3).

3 EXPERIMENTAl RESULTS

Two experiments are conducted to validate the effectiveness of the proposed method. One uses IKONOS MS and Pan images, and the other uses Quickbird Pan and MS images. The Quickbird images are available at the Global Land Cover Facility (GLCF) at the University of Maryland (2005).

Because of the limit of the experiment condition, there are no ideal high resolution MS images as reference to evaluate performance of the fusion methods. In order to asses the spectral and spatial quality of the fused images, we work with spatially degraded images. The original IKONOS (Quickbird) satellite MS and Pan images are degraded to 16m (9.76m) and 4m (2.44m), respectively, and the original MS images are used as reference images (As can be seen in Fig. 2(a) to (c) and Fig. 3(a) to (c)).

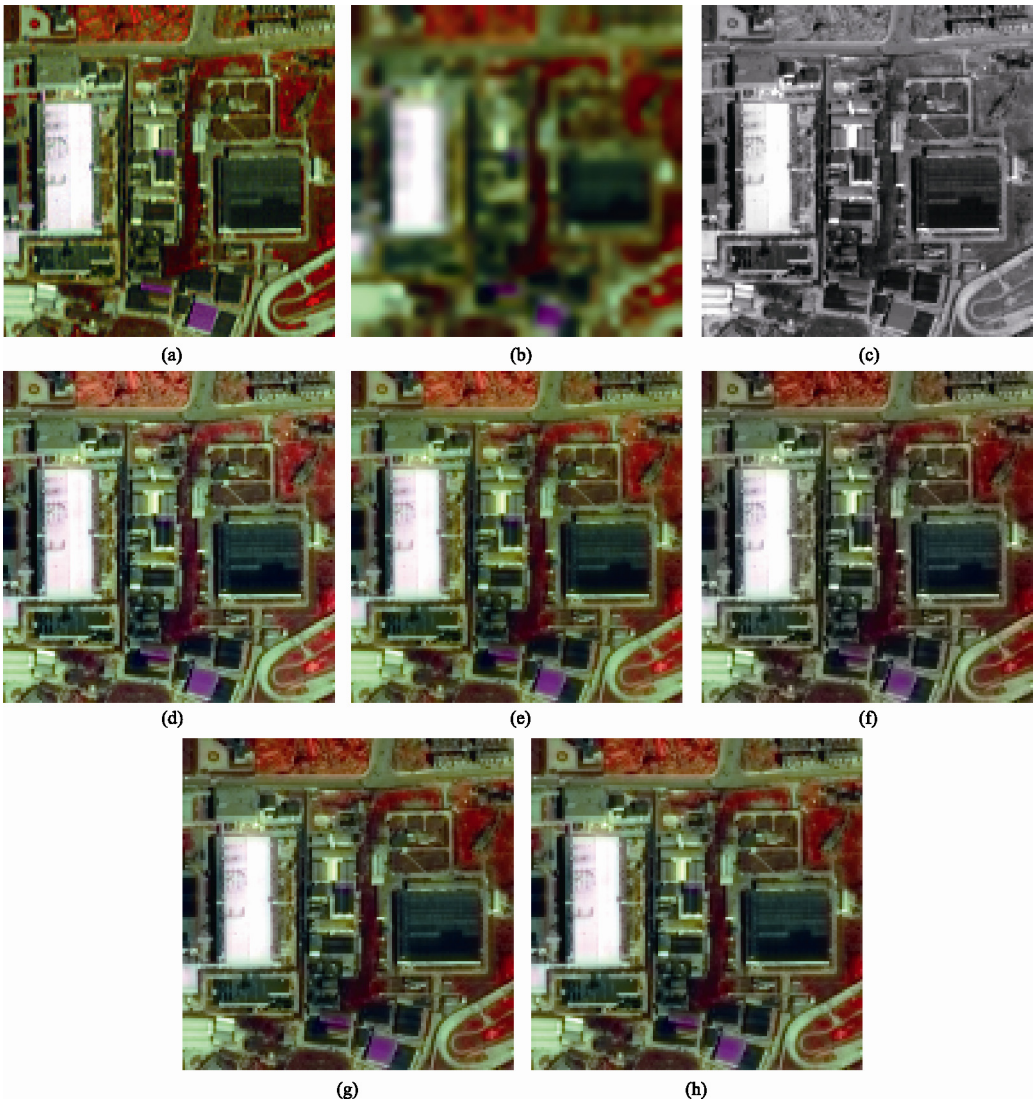

Fig. 2 Fusion results from the degraded bands 4, 2 and 1 images shown as a color composite (IKONOS data set). In order to compare and analyze, the shown images are part of the original images and be magnified

(a) Original MS images; (b) Degraded MS images; (c) Degraded Pan image. (d) Fused MS images using the GIHS method. (e) Fused MS images using the Choi method. (f) Fused MS images using the atrWT method. (g) Fused MS images using the atrWT+GIHS method. (h) Fused MS images using the proposed method

(C)1994-2021 China Academic Journal Electronic Publishing House. All rights reserved. http://www.cnki.net

In order to compare the performance of the fusion methods, the following evaluation parameters are adopted:

(1) spectral correlation coefficient (CC)

CC is the correlation coefficient between the band of the fused images and corresponding band of original MS image. The more spectral information the fusion results keep, the more the value of CC is close to 1, and the ideal value of CC is 1.

(2) relative global dimensional synthesis error

The lower the ERGAS value, the higher the spectral quality of the fused images. The best value of ERGAS is 1.

(3) spatial correlation coefficient (sCC)

This paper adopts the Zhou et al.'s method (1998). The larger the value of sCC is, the more spatial detail information are injected into MS images.

The compared fusion methods are Tu's GIHS fusion method, Choi's trade-off fusion method (the value of trade-off is set to 7), the fusion method based on atrous wavelet transform (atrWT), which is also called undecimated wavelet transformation and the fusion method based on atrous wavelet transform combined with GIHS method (atrWT+GIHS). In the implementation of wavelet transformation, the biorthogonal tight support spline wavelet are adopted (corrsponding the function 'bior2.2' in Matlab software), the decomposition level is set to 3. Because of the shift-invariance of the atrous wavelet transform, thus the performance of the fusion results is better with the wavelet fusion methods.

For the fusion of IKONOS imagery, the selected parameters for the proposed method are as follows: α=0.01, β=1, γ=0.3, q=10^{-8}, the maximum number of iterations K=16, and the Gaussian kernel $\mathbf{C}=\begin{bmatrix} 0 & -0.25 & 0 \\ -0.25 & 1 & -0.25 \\ 0 & -0.25 & 0 \end{bmatrix}$.

For the fusion of Quickbird imagery, the selected parameters for the proposed method are as follows: α=0.01, β=1, γ=0.16, q=10^{-6}, the maximum number of iterations K=16, and the Gaussian kernel **C** be the same as used in IKONOS imagery experiment.

The fusion results of all methods are shown in Fig. 2 (d) to (h) and Fig. 3 (d) to (h). From the visual point of view, the fusion

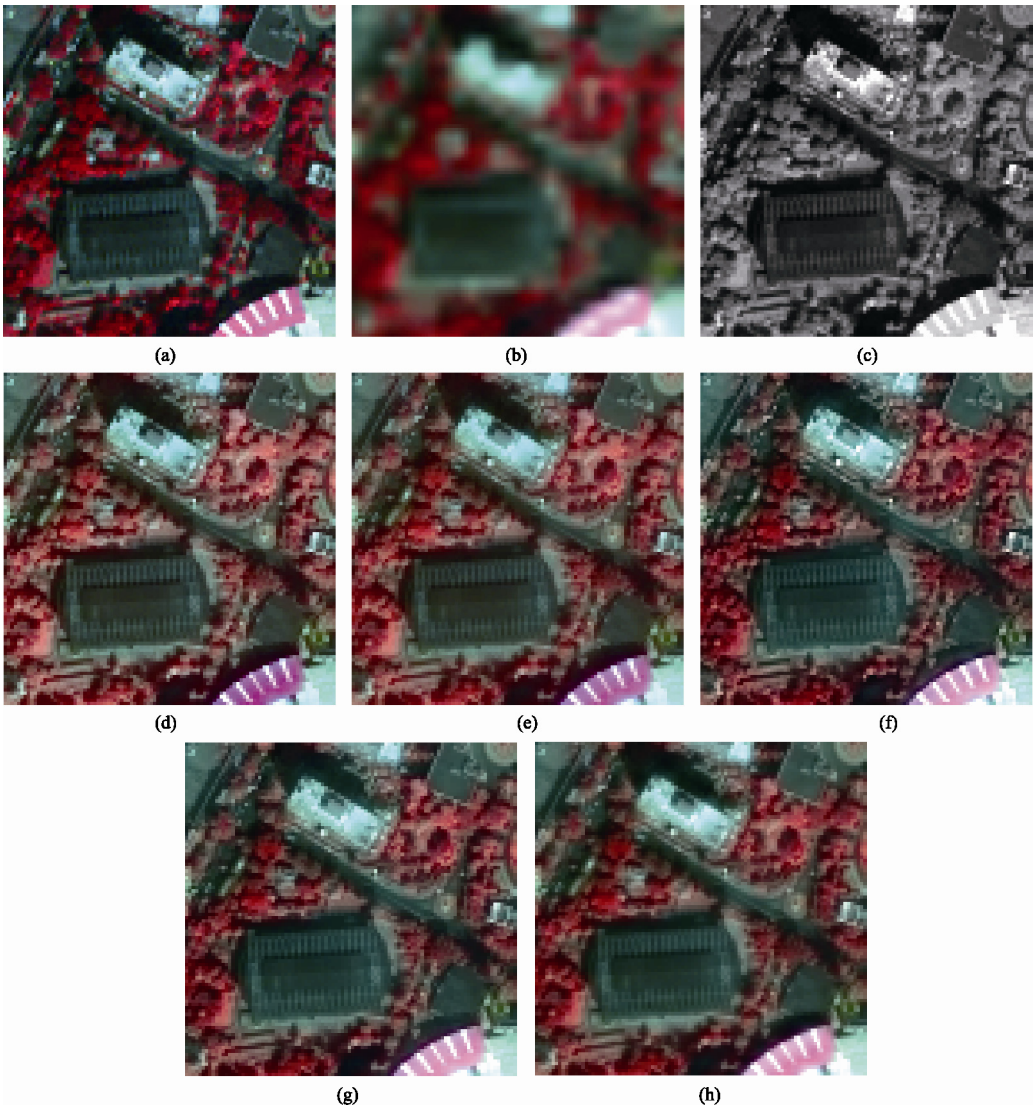

Fig. 3 Fusion results from the degraded bands 4, 3 and 2 images shown as a color composite (Quickbird data set). In order to compare and analyze, the shown images are part of the original images and be magnified

(a) Original MS images. (b) Degraded MS images. (c) Degraded Pan image. (d) Fused MS images using the GIHS method. (e) Fused MS images using the Choi's method. (f) Fused MS images using the atrWT method. (g) Fused MS images using the atrWT+GIHS method. (h) Fused MS images using the proposed method

(C)1994-2021 China Academic Journal Electronic Publishing House. All rights reserved. http://www.cnki.net

results of all fusion methods are better than the degraded MS imagery in spectral and spatial information (As can be seen from Fig. 2(b) and Fig. 3(b)), this shows the proposed method and other fusion methods improve the quality of the fused images. Although there are no perceptible differences between spectral quality of the fused images when we compared our proposed method with the atrWT method and the atrWT+GIHS method. But our proposed method has slightly better spectral quality than the GISH fusion method and Choi's method.

Compared with the degraded MS images (as can be seen from Fig. 2(b) and Fig. 3(b)), the spatial detail information of the fused images using each fusion method is improved greatly. This shows that the spatial detail information is effectively injected into MS images. Spatial detail information of Fig. 2 (d) to (h) and Fig. 3 (d) to (h) is not obviously distinguished visually.

The objective evaluation of spectral and spatial quality for the fusion results of all fusion methods are as follows:

The comparison of the spectral quality is given in Table 1 and Table 2. From Table 1 and Table 2, we can see that the value of CC and the mean of CC ($\overline{CC}$) of the proposed method are larger than the degraded image. This shows that the proposed method improves the spectral quality of the fused images. For the proposed method, the CC value of the NIR band is slightly lower than that of the atrWT+IHS method. The $\overline{CC}$ value for the proposed method is the maximum for all fusion methods. Besides, the ERGAS value for the proposed method is the minimum for all fusion methods. This shows that the proposed method have better spectral quality than the existing fusion methods.

From Table 3 and Table 4, we can see that the fused images of each method have better spatial quality than the degraded images. The proposed method have slightly better performance than Choi's method (trade-off parameters), and slightly inferior performance when compared to GIHS method, atrWT methods and atrWT+GIHS method.

Table 1 Spectral quality comparison of the fusion results using the IKONOS images

Project		Degraded	GIHS	Choi	atrWT	atrWT+GIHS	Proposed	Ideal
CC	NIR	0.8703	0.9554	0.9516	0.9598	0.9583	0.9601	1
	R	0.8278	0.9466	0.9475	0.9449	0.9520	0.9557	1
	G	0.8681	0.9589	0.9641	0.9623	0.9659	0.9694	1
	B	0.9361	0.9369	0.9562	0.9558	0.9614	0.9620	1
$\overline{CC}$		0.8756	0.9495	0.9548	0.9557	0.9594	0.9618	0
ERGAS		2.0143	1.3619	1.3595	1.2167	1.1895	1.1607	0

Table 2 Spectral quality comparison of the fusion results using the Quickbird images

Project		Degraded	GIHS	Choi	atrWT	atrWT+GIHS	Proposed	Ideal
CC	NIR	0.8908	0.9369	0.9396	0.9571	0.9699	0.9652	1
	R	0.8925	0.8773	0.9128	0.9357	0.9373	0.9497	1
	G	0.8954	0.8958	0.9288	0.9455	0.9464	0.9587	1
	B	0.9194	0.8836	0.9213	0.9348	0.9361	0.9506	1
$\overline{CC}$		0.8995	0.8984	0.9256	0.9433	0.9474	0.9560	0
ERGAS		1.8836	1.9807	1.7875	1.4456	1.3998	1.2776	0

Table 3 Spatial quality comparison of the fusion results using the IKONOS images

project		Degraded	GIHS	Choi	atrWT	atrWT+IHS	proposed	Ideal
sCC	NIR	0.7318	0.9860	0.9740	0.9973	0.9873	0.9844	1
	R	0.7323	0.9940	0.9844	0.9920	0.9935	0.9918	1
	G	0.7329	0.9835	0.9694	0.9823	0.9834	0.9806	1
	B	0.7308	0.9867	0.9742	0.9860	0.9868	0.9846	1
$\overline{sCC}$		0.7319	0.9876	0.9755	0.9894	0.9877	0.9853	1

Table 4 Spatial quality comparison of the fusion results using the Quickbird images

project		Degraded	GIHS	Choi	atrWT	atrWT+IHS	proposed	Ideal
sCC	NIR	0.2385	0.9765	0.9593	0.9932	0.9819	0.9693	1
	R	0.2104	0.9952	0.9892	0.9868	0.9892	0.9859	1
	G	0.2113	0.9939	0.9853	0.9862	0.9885	0.9831	1
	B	0.2017	0.9950	0.9896	0.9872	0.9897	0.9862	1
$\overline{sCC}$		0.2155	0.9902	0.9808	0.9883	0.9873	0.9811	1

(C)1994-2021 China Academic Journal Electronic Publishing House. All rights reserved. http://www.cnki.net

Considering the proposed method has the best spectral quality compared with the other fusion methods (As can be seen in Table 1 and Table 2), and that the key problem of the fusion of the MS and Pan images is to improve spatial detail while keep the spectral information of the original MS image, this shows that the proposed method is effective.

4 CONCLUSION

This paper proposes a new fusion method by combining GIHS and MAP framework based on spectral characteristics of a new type of remote sensing platforms. The proposed method has the main feature of improved spatial details while keeps the spectral information of original MS images by imposing constrains on the intensity component and Pan image based on MAP. For IKONOS imagery and Quickbird imagery experiments, it shows that the proposed method is effective in holding the spectral information of the original MS images. Each constraint parameters is chosen according by the trial and error method for the MAP estimation using an iteration optimization algorithm. Adaptive selection of those parameters would be an important future work.

REFERENCES

Choi M. 2006. A new intensity-hue-saturation fusion approach to image fusion with a tradeoff parameter. *IEEE Transactions on Geoscience and Remote Sensing*, **44** (6): 1672—1682

Gonzalez-Audicana M, José L S and Raquel G C. 2004. Fusion of multispectral and panchromatic images using improved IHS and PCA merges based on wavelet decomposition. *IEEE Trasnsactions on Geoscience and Remote Sensing*, **42**(6): 1291—1299

Gonzalez-Audicana M, Otazu X, Fors O and Alvarez-Mozos J. 2006. A low computational-cost method to fuse IKONOS images using the spectral response function of its sensors. *IEEE Transactions on Geoscience and Remote Sensing*, **44**(6): 1683—1691

IKONOS Relative Spectral Response of GeoEye Corporation. 2008. http://www.geoeye.com/CorpSite/resource/white-papers.aspx.

Li X, He M Y, Michel R and Wei B G. 2009. A new algorithm for fusing very high resolution remote sensing images. *Journal of Electronics & Information Technology*, **31**(12): 2886—2891

Mohamed E and Mohammad A. 2008. Superresolution construction of multispectral imagery based on local enhancement. *IEEE Geoscience and Remote Sensing Letters*, **5**(2): 276—279

Pohl C and Van Genderen J L. 1998. Multisensor image fusion in remote sensing:concepts,methods and applications. *International Journal of Remote Sensing*, **19**(5): 823—854

QuickBird Imagery of the Global Land Cover Facility (GLCF) at the University of Maryland. 2005. http://www.landvover.org/data/quickbird

Shah V P, Younan N H and King R L. 2008. An efficient Pan-sharpening method via a combined adaptive PCA approach and Contourlets. *IEEE Transactions on Geoscience and Remote Sensing*, **46**(5): 1323—1335

Song H H, Yu S Y, Song L and Yang X K. 2007. Fusion of multispectral and panchromatic satellite images based on contourlet transform and local averge gradient. *Optical Engineering*, **46** (2): 020502

Thomas C, Ranchin T, Wald L and Chanussot J. 2008. Synthesis of multispectral images to high spatial resolution: a critical review of fusion methods based on remote sensing physics. *IEEE Transactions on Geoscience and Remote Sensing*, **46**(5): 1301—1312

Tu T M, Huang P S, Hung C L and Chang C P. 2004. A fast intensity-hue-saturation fusion technique with spectral adjustment for IKONOS imagery. *IEEE Geoscience and Remote Sensing Letters*, **1**(4) : 309—312

Xu J, Guan Z Q, He X F and Hu J W. 2009. Novel method for merging panchromatic and multi-spectral images based on sensor spectral response. *Journal of Remote Sensing*, **13**(1): 97—102

Zhou J, Civco D L and Silander J A. 1998. A wavelet transform method to merge Landsat TM and SPOT panchromatic data. *International Journal of Remote Sensing*, **19**(4):743—757

(C)1994-2021 China Academic Journal Electronic Publishing House. All rights reserved. http://www.cnki.net

联合 IHS 变换和 MAP 估计的遥感图像融合

石爱业, 徐立中, 汤 敏

河海大学 计算机与信息学院, 江苏 南京 210098

摘 要: 为了提高多光谱图像和全色图像的融合质量, 提出一种基于推广的 IHS(Generalized Intensity-Hue-Saturation, GIHS)变换与最大后验概率 MAP(Maximum a Posteriori)相结合的遥感图像融合算法。该算法首先经过 GIHS 变换, 由多光谱图像得到强度分量; 其次针对强度分量和全色图像, 通过 MAP 构建高分辨率图像的成像模型, 采用最速下降优化算法得到富含光谱信息的高分辨率全色图像; 进而依据 GIHS 变换得到融合图像。实验中分别以 IKONOS 卫星、Quickbird 卫星的多光谱图像和全色图像为例, 进行融合算法验证, 并与 GIHS 融合算法、传统的小波变换融合算法、小波变换结合 IHS 变换的融合算法等进行比较分析, 实验表明, 新的融合方法具有更好的融合效果。

关键词: 图像融合, 小波变换, MAP, IHS 变换

中图分类号: TP751 **文献标志码:** A

引用格式: 石爱业, 徐立中, 汤 敏. 2010. 联合 IHS 变换和 MAP 估计的遥感图像融合. 遥感学报, **14**(6): 1259—1272
Shi A Y, Xu L Z and Tang M. 2010. Remotely-sensed image fusion based on generalized IHS transformation and MAP analysis. *Journal of Remote Sensing*. **14**(6): 1259—1272

1 引 言

针对诸如 IKONOS 等新型的高分辨率卫星, 如何通过有效的图像融合方法, 来融合其上的多光谱(Multispectral, MS)图像和全色(Panchromatic, Pan)图像, 以使融合的图像既保留 Pan 图像的纹理细节, 又保持 MS 图像的光谱信息, 将是十分必要的。常用的遥感图像融合方法主要有: 通用的分量替换融合方法与基于多分辨分析的融合方法 (Choi, 2006; González-Audícana 等, 2004, 2006; Li 等, 2009; Mohamed & Mohammad, 2008; Pohl & Van Genderen, 1998; Shah 等, 2008; Tomas 等, 2008; Tu 等, 2004; Xu 等, 2009; Zhou 等, 1998)。

通用的分量替换融合方法中最常用的融合方法之一是 IHS 融合方法, 其空间分辨率增强较好, 但是融合图像的光谱质量不高。针对 IHS 融合方法存在的光谱失真问题, Tu 等人以线性 IHS 变换为基础提出一种推广的 IHS 变换(GIHS)融合方法(Tu 等, 2004), MS 图像的强度分量 I 由红(R)波段、绿(G)波段、蓝(B)波段以及近红外(NIR)波段的 4 个波段的 DN(digital number)值的平均值构成, 该融合方法的主要特点无需进行 IHS 逆变换, 融合过程就是 MS 图像、Pan 图像和 I 分量之间的加减运算, 故此减少了融合的计算代价, 但是融合图像的光谱失真依然较大, 只是部分改善。

针对 IHS/GIHS 融合方法的不足, Choi (2006) 以 GIHS 融合方法为基础, 在融合过程中, 采用平衡参数的快速融合方法, 通过调节平衡参数来控制融合图像的光谱质量和空间细节质量。该方法的主要不足之处在于无法确定最优的平衡参数 (Tomas 等, 2008)。González-Audícana 等 (2006) 基于传感器的光谱响应函数, 结合 GIHS 研究了一种快速遥感图像融合方法, 但是该方法在构建遥感器的光谱响应函数时, 参数的选择需要根据经验估计, 且该方法仅对 IKONOS 的 MS 和 Pan 图像的融合进行了算法的验证。

基于多分辨分析的融合方法中, 最常用的是基于小波变换融合方法, 其在遥感图像的融合中得到广泛地运用 (Pohl & Van Genderen, 1998; Zhou, 1998; Tomas 等, 2008), 但是由于其只具有水平、垂直、对

收稿日期: 2010-01-15; 修订日期: 2010-04-18

基金项目: 国家自然科学基金(编号: 60774092、60872096、60901003); 高等学校博士学科点专项科研基金(编号: 20070294027)。

第一作者简介: 石爱业(1969—), 男, 博士, 讲师, 2009 年毕业于河海大学计算及信息工程学院, 目前主要从事遥感图像处理的研究工作, 发表论文十余篇。E-mail: ayshi.hhu@gmail.com。

(C)1994-2021 China Academic Journal Electronic Publishing House. All rights reserved. http://www.cnki.net

角 3 个有限的方向, 不能“最优”的表示含有线或面奇异的二维图像。针对此, Contourlet 变换被引入遥感图像的融合中, 改善了遥感图像的融合性能(Song 等, 2007), 但是由于 Contourlet 变换的多方向性, 该类融合算法计算复杂度很大 (Shah 等, 2008)。

IHS 变换结合小波变换的融合方法也在遥感图像融合中得到应用 (González-Audícana 等, 2004), 其原理为: 先利用小波变换来融合 MS 图像的强度分量和 Pan 图像, 得到一个新的强度分量, 然后再做 IHS 逆变换得到融合图像。由于该方法将小波变换融合的优点和 IHS 变换融合的优点相结合, 故此融合图像的质量较好。

为了更好的提高融合图像的质量, 该文在 GIHS 融合方法的基础上, 针对新型高分辨率遥感数据, 提出一种基于 MAP 的遥感图像融合方法, 主要依据是: MAP 估计可以嵌入先验知识, 并且能够对 MS 图像的强度分量和 Pan 图像施加一定的限制条件来约束解的范围, 从而使得最终的融合图像在空间细节信息的增强与光谱信息的保持两个方面的综合性能得到提高。

2 基于 GIHS 与 MAP 相结合的遥感图像融合新算法

2.1 GIHS 融合方法

针对 IKONOS 的 MS 图像和 Pan 图像的融合, 考虑到其全色波段的光谱范围覆盖了红波段、绿波段、蓝波段以及近红外波段 4 个波段, Tu 等 (2004) 将近红外波段(NIR)图像引入到强度分量的计算中, 采用 GIHS 来克服光谱失真。设 $X \in \{\text{NIR}, R, G, B\}$, 则有下述融合结果:

$$\boldsymbol{F}_X = \boldsymbol{M}_X^{\text{upsample}} + (\boldsymbol{P} - \boldsymbol{I}_{\text{g}}) \tag{1}$$

式中, $\boldsymbol{F}_X$ 表示第 X 波段的融合图像, $\boldsymbol{P}$ 表示原始 Pan 图像, $\boldsymbol{M}_X$ 表示原始低分辨率 MS 图像的 X 波段图像, $\boldsymbol{M}_X^{\text{upsample}}$ 表示原始低分辨率 MS 图像的 X 波段的上采样图像(放大倍数为 4), $\boldsymbol{I}_g$ 表示上采样的 MS 图像的强度分量, 其定义为:

$$\boldsymbol{I}_{\text{g}}=\frac{1}{4}\sum_{X\in\{\text{NIR},R,G,B\}}\boldsymbol{M}_X^{\text{upsample}} \tag{2}$$

由式(1)可见, GIHS 融合方法中将 MS 图像中的 NIR 波段引入到强度分量 $\boldsymbol{I}_{\text{g}}$ 的计算中, 虽然可以在一定程度上克服融合图像的光谱失真, 但是融合图像的光谱失真问题依然存在, 融合性能还有待进一步提高。

针对上述存在的问题, 本文提出基于 GIHS 的 MAP 统计融合方法, 来得到一个新的高分辨率图像 $\boldsymbol{i}_{\text{new}}$ 来替代式(1)中的 Pan 图像 $\boldsymbol{P}$, 即

$$\boldsymbol{F}_X = \boldsymbol{M}_X^{\text{upsample}} + \left(\boldsymbol{i}_{\text{new}} - \boldsymbol{I}_{\text{g}}\right) \tag{3}$$

式中, $\boldsymbol{i}_{\text{new}}$ 在 MAP 框架下, 通过组合 MS 图像的强度分量 $\boldsymbol{I}_{\text{g}}$ 和 Pan 图像所得的高分辨率图像, 可使最终的融合图像在保持原始 MS 图像的基础上, 提高融合图像的空间分辨率。下面阐述如何利用 MAP 方法估计高分辨率图像 $\boldsymbol{i}_{\text{new}}$。

2.2 MAP 估计算法

新算法先基于观测模型推导出高分辨率图像 $\boldsymbol{i}_{\text{new}}$ 和原始低分辨率 MS 图像的强度分量图像以及 Pan 图像的 MAP 框架, 然后再利用梯度下降优化算法得出估计的 $\boldsymbol{i}_{\text{new}}$ 图像。该文主要研究 IKONOS 卫星的 MS 图像和 Pan 图像融合、Quickbird 卫星的 MS 图像和 Pan 图像的融合。不失一般性, 以 IKONS 卫星的图像融合对新算法进行阐述。

2.2.1 观测模型

设理想的高分辨率 MS 图像为 $\boldsymbol{z}$, 其 NIR、R、G、B 波段的 DN 值分别为: $\boldsymbol{z}_{\text{NIR}}$, $\boldsymbol{z}_R$, $\boldsymbol{z}_G$, $\boldsymbol{z}_B$。四个波段的噪声分别为 n_{NIR}, n_R, n_G, n_B, 假设各波段噪声均是独立同分布的高斯随机噪声, 波段均值为 0, 四个波段的方差分别为 β_{NIR}^{-1}, β_R^{-1}, β_G^{-1}, β_B^{-1}, 则

$$p(\boldsymbol{n}_X)=\frac{1}{(2\pi)^{M/2}(1/\beta_X)^{M/2}}\times \exp\left\{-\frac{1}{2}\beta_X\sum(\boldsymbol{n}_X\odot\boldsymbol{n}_X)\right\} \tag{4}$$

式中, $\odot$ 表示两个图像矩阵逐点相乘的算子。

理想的高分辨率 MS 图像 X 波段($X\in$ {NIR, R, G, B})的退化模型可以表示为:

$$\boldsymbol{M}_X = \boldsymbol{W}\boldsymbol{z}_X + \boldsymbol{n}_X \tag{5}$$

式中, $\boldsymbol{z}_X$ 表示理想的高分辨率 MS 图像的第 X 波段图像, $\boldsymbol{W}$ 表示遥感成像系统的点扩散函数, 其可以看作模糊及下采样操作, 即 $\boldsymbol{W}$=$\boldsymbol{D}\boldsymbol{H}$, 其中 $\boldsymbol{D}$ 表示在图像的行和列方向进行 4 抽 1 的下采样操作, $\boldsymbol{H}$ 可以近似为 (Mohamed & Mohammad, 2008): $\boldsymbol{H}=\frac{1}{16}\boldsymbol{I}_4$, $\boldsymbol{I}_4$ 为 4×4 的全 1 矩阵。

由式(5), 得:

$$\frac{1}{4}\sum_{X\in\{\text{NIR},R,G,B\}}\boldsymbol{M}_X=\frac{1}{4}\boldsymbol{W}\sum_{X\in\{\text{NIR},R,G,B\}}\boldsymbol{z}_X+\frac{1}{4}\sum_{X\in\{\text{NIR},R,G,B\}}\boldsymbol{n}_X \tag{6}$$

将式(6)写做

(C)1994-2021 China Academic Journal Electronic Publishing House. All rights reserved. http://www.cnki.net

$$\boldsymbol{I}_l = \boldsymbol{W}\boldsymbol{i}_{\text{new}} + \boldsymbol{n} \tag{7}$$

式中，$\boldsymbol{I}_l = \frac{1}{4}\sum_{X\in\{\text{NIR},R,G,B\}} \boldsymbol{M}_X$，$\boldsymbol{i}_{\text{new}} = \frac{1}{4}\sum_{X\in\{\text{NIR},R,G,B\}} \boldsymbol{z}_X$，$\boldsymbol{n} = \frac{1}{4}\sum_{X\in\{\text{NIR},R,G,B\}} \boldsymbol{n}_X$

式中，高斯随机噪声 $\boldsymbol{N}$ 均值为 0，方差为 β^{-1}（与 β_{NIR}^{-1}，β_R^{-1}，β_G^{-1}，β_B^{-1} 相关）。

另外理想的高分辨率 MS 图像和 Pan 图像 $\boldsymbol{P}$ 间有：

$$\boldsymbol{P} = \sum_{X\in\{\text{NIR},R,G,B\}} \lambda_X \boldsymbol{z}_X + \boldsymbol{v} \tag{8}$$

式中，假设 $\boldsymbol{v}$ 为 0 均值、方差为 γ^{-1} 的高斯随机噪声，λ_X($X\in$ {NIR, R, G, B})表示待求的理想高分辨率图像 X 波段对高分辨率 Pan 图像的加权系数。

针对 IKONOS，由其光谱响应曲线见图 1 (美国 GeoEye 公司，2008)，MS 图像 4 个波段所占的波谱宽度近似为 Pan 图像波谱宽度的 1/4，故可以做如下近似：

$$\lambda_{\text{NIR}} = \lambda_R = \lambda_G = \lambda_B = 1/4 \tag{9}$$

故此式(8)又可以写为：

$$\boldsymbol{P} = \boldsymbol{i}_{\text{new}} + \boldsymbol{v} \tag{10}$$

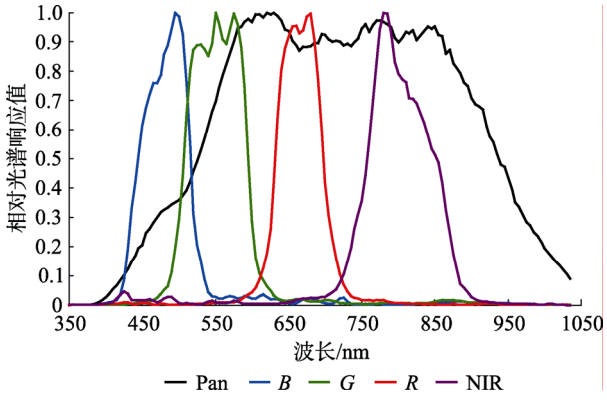

图 1 IKONOS 的相对光谱响应曲线

2.2.2 MAP 估计

MAP 估计就是要寻找一个新的 Pan 图像 $\boldsymbol{i}_{\text{new}}$ 以使下式的条件概率最大化：

$$\hat{\boldsymbol{i}}_{\text{new}} = \arg\max_{\boldsymbol{i}_{\text{new}}} \left[\Pr_{\boldsymbol{i}_{\text{new}}|\boldsymbol{I}_l,\boldsymbol{P}}(\boldsymbol{i}_{\text{new}} \mid \boldsymbol{I}_l, \boldsymbol{P})\right] \tag{11}$$

应用 Bayes 准则，上式可以表述为：

$$\hat{\boldsymbol{i}}_{\text{new}} = \arg\max_{\boldsymbol{i}_{\text{new}}} \frac{\Pr_{\boldsymbol{I}_l,\boldsymbol{P}|\boldsymbol{i}_{\text{new}}}(\boldsymbol{I}_l, \boldsymbol{P} \mid \boldsymbol{i}_{\text{new}})\Pr(\boldsymbol{i}_{\text{new}})}{\Pr(\boldsymbol{I}_l, \boldsymbol{P})} \tag{12}$$

因为上式的分母与 $\boldsymbol{i}_{\text{new}}$ 无关，所以式(12)又可以描述为：

$$\hat{\boldsymbol{i}}_{\text{new}} = \arg\max_{\boldsymbol{i}_{\text{new}}} \Pr_{\boldsymbol{I}_l,\boldsymbol{P}|\boldsymbol{i}_{\text{new}}}(\boldsymbol{I}_l, \boldsymbol{P} \mid \boldsymbol{i}_{\text{new}})\Pr(\boldsymbol{i}_{\text{new}}) = \arg\max_{\boldsymbol{i}_{\text{new}}} \Pr_{\boldsymbol{I}_l|\boldsymbol{i}_{\text{new}}}(\boldsymbol{I}_l \mid \boldsymbol{i}_{\text{new}})\Pr_{\boldsymbol{p}|\boldsymbol{i}_{\text{new}}}(\boldsymbol{P} \mid \boldsymbol{i}_{\text{new}})\Pr(\boldsymbol{i}_{\text{new}}) \tag{13}$$

假定上述的 $\Pr(\boldsymbol{i}_{\text{new}})$ 服从同步自回归模型，也即 $\Pr(\boldsymbol{i}_{\text{new}}) \propto \exp\left\{-\frac{1}{2}\alpha\|\boldsymbol{C}\boldsymbol{i}_{\text{new}}\|^2\right\}$，其中 $\boldsymbol{C}$ 为高斯核。再依据式(7)、式(10)，则关于 $\boldsymbol{i}_{\text{new}}$ 的 MAP 估计可以描述为：

$$\hat{\boldsymbol{i}}_{\text{new}} = \arg\min_{\boldsymbol{i}_{\text{new}}} L(\boldsymbol{i}_{\text{new}}) = \arg\min_{\boldsymbol{i}_{\text{new}}} \left(\frac{1}{2}\beta\|\boldsymbol{I}_l - \boldsymbol{W}\boldsymbol{i}_{\text{new}}\|_2^2 + \frac{1}{2}\gamma\|\boldsymbol{P} - \boldsymbol{i}_{\text{new}}\|_2^2 + \frac{1}{2}\alpha\|\boldsymbol{C}\boldsymbol{i}_{\text{new}}\|_2^2\right) \tag{14}$$

上式中第一项约束重建图像对原始低分辨率 MS 图像强度分量的失真度，第二项约束重建图像对 Pan 图像的失真度，而第三项则约束重建图像的平滑度。通过对参数 α、β、γ 的适当选取可以使得重建的图像 $\boldsymbol{i}_{\text{new}}$ 既保有原始 MS 图像的光谱信息，又具有 Pan 图像的空间细节信息。

2.2.3 梯度下降优化算法

考虑到优化算法的复杂度，采用简单的梯度下降算法来求解最终的高分辨率图像 $\boldsymbol{i}_{\text{new}}$。式(14)中的代价函数关于 $\boldsymbol{i}_{\text{new}}$ 的梯度为：

$$g(\boldsymbol{i}_{\text{new}}) = \frac{\partial L(\boldsymbol{i}_{\text{new}})}{\partial \boldsymbol{i}_{\text{new}}} = \beta\boldsymbol{W}^{\text{T}}(\boldsymbol{W}\boldsymbol{i}_{\text{new}} - \boldsymbol{I}_l) + \gamma(\boldsymbol{i}_{\text{new}} - \boldsymbol{P}) + \alpha\boldsymbol{C}^{\text{T}}\boldsymbol{C}\boldsymbol{i}_{\text{new}} \tag{15}$$

高分辨率图像估计 $\hat{\boldsymbol{i}}_{\text{new}}$ 的更新算法如下：

$$\hat{\boldsymbol{i}}_{\text{new}}^{k+1} = \hat{\boldsymbol{i}}_{\text{new}}^{k} - \varepsilon^k g(\boldsymbol{i}_{\text{new}})|_{\boldsymbol{i}_{\text{new}}=\hat{\boldsymbol{i}}_{\text{new}}^k} \tag{16}$$

式(16)中的参数 ε^k 表示第 k 次迭代的步长。该参数选择既要保证足够小，以防止扩散，又要保证足够大，以保证在适当的迭代之后收敛。优化的迭代步长可以由下式的最小化而得：

$$L\left(\hat{\boldsymbol{i}}_{\text{new}}^{k+1}\right) = L\left(\hat{\boldsymbol{i}}_{\text{new}}^{k} - \varepsilon^k g(\boldsymbol{i}_{\text{new}})|_{\boldsymbol{i}_{\text{new}}=\hat{\boldsymbol{i}}_{\text{new}}^k}\right) \tag{17}$$

式(17)对 ε^k 求导，并令求导结果为 0，可以求解步长如下：

$$\varepsilon^k = \frac{\beta\sum\left[\xi\odot\left(\boldsymbol{W}\hat{\boldsymbol{i}}_{\text{new}}^k - \boldsymbol{I}_l\right)\right] + \alpha\sum\left[\psi\odot\boldsymbol{C}\hat{\boldsymbol{i}}_{\text{new}}^k\right] + \gamma\sum\left[g\left(\hat{\boldsymbol{i}}_{\text{new}}^k\right)\odot\left(\hat{\boldsymbol{i}}_{\text{new}}^k - \boldsymbol{P}\right)\right]}{\beta\sum[\xi\odot\xi] + \alpha\sum[\psi\odot\psi] + \gamma\sum\left[g\left(\hat{\boldsymbol{i}}_{\text{new}}^k\right)\odot g\left(\hat{\boldsymbol{i}}_{\text{new}}^k\right)\right]} \tag{18}$$

式中，$\odot$ 表示两个图像矩阵逐点相乘的算子，$\xi = \boldsymbol{W}g\left(\hat{\boldsymbol{i}}_{\text{new}}^k\right)$，$\psi = \boldsymbol{C}g\left(\hat{\boldsymbol{i}}_{\text{new}}^k\right)$

(C)1994-2021 China Academic Journal Electronic Publishing House. All rights reserved. http://www.cnki.net

2.3 新算法的实现步骤

新的融合算法实现步骤描述如下:

步骤 **1** 根据 GIHS, 求得低分辨率 MS 图像的强度分量图像 $\boldsymbol{I}_I$。

步骤 **2** 设置迭代次数 k=0, 给定预设的上界值 q。对低分辨率 MS 图像进行双三次插值, 并依据 GIHS 的定义, 求取 i_{new}^0。

步骤 **3** 依据式(15)计算梯度 $g(\boldsymbol{i}_{\text{new}})|_{\boldsymbol{i}_{\text{new}}=\hat{\boldsymbol{i}}_{\text{new}}^k}$。

步骤 **4** 根据式(16)、式(18)计算 $\hat{i}_{\text{new}}^{k+1}$。

步骤 **5** 若 $\left\|\hat{\boldsymbol{i}}_{\text{new}}^{k+1}-\hat{\boldsymbol{i}}_{\text{new}}^{k}\right\|^2 \Big/ \left\|\hat{\boldsymbol{i}}_{\text{new}}^{k}\right\|^2 \leqslant q$ 或达到设定的迭代次数, 停止循环并转到步骤 7。

步骤 **6** 使得 k=k+1, 回到步骤 3。

步骤 **7** 根据式(2)得到融合图像。

3 实验与结果分析

为了验证所提算法的有效性, 共做两组实验。一组以 IKONOS 卫星的 MS 图像和 Pan 图像的融合为研究对象, 另一组以 Quickbird 卫星的 MS 图像和 Pan 图像的融合为研究对象。实验中所采用的 Quickbird 图像数据来源于美国马里兰大学的 GLCF(Global Land Cover Facility, 2005)。

由于实验条件限制, 没有理想的 MS 图像作为参考图像, 来衡量融合算法的性能。为评估融合图像的光谱质量和空间细节质量, 将 IKONOS (Quickbird)卫星的原始 MS 图像和 Pan 图像的空间分辨率分别退化到 16m(9.76m)和 4m(2.44m)作为实验数据, 原始 MS 图像做参考图像(分别见图 2(a)—(c)、图 3(a)—(c))。

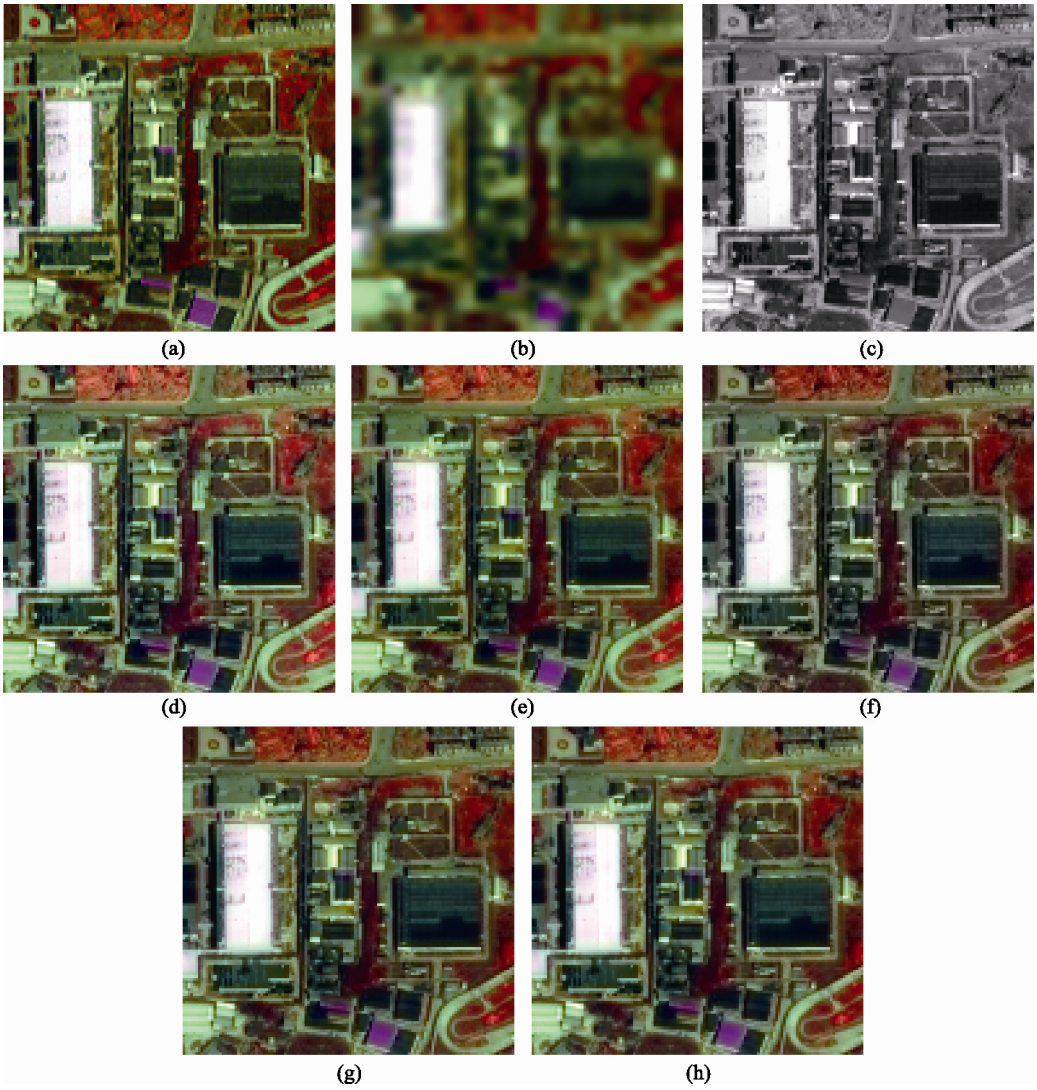

图 2 IKONOS 图像融合结果, 所有 MS 图像是 4、2、1 波段的假彩色合成图(为了更好的分析比较, 所有显示的图像只是原融合图像的一部分, 且进行了放大处理)

(a) 原始 MS 图像; (b) 降质的 MS 图像; (c) 降质的 Pan 图像; (d) GIHS 方法融合的图像; (e) Choi 方法融合的图像; (f) atrWT 方法融合的图像; (g) atrWT+GIHS 方法融合的图像; (h) 新方法融合的图像

(C)1994-2021 China Academic Journal Electronic Publishing House. All rights reserved. http://www.cnki.net

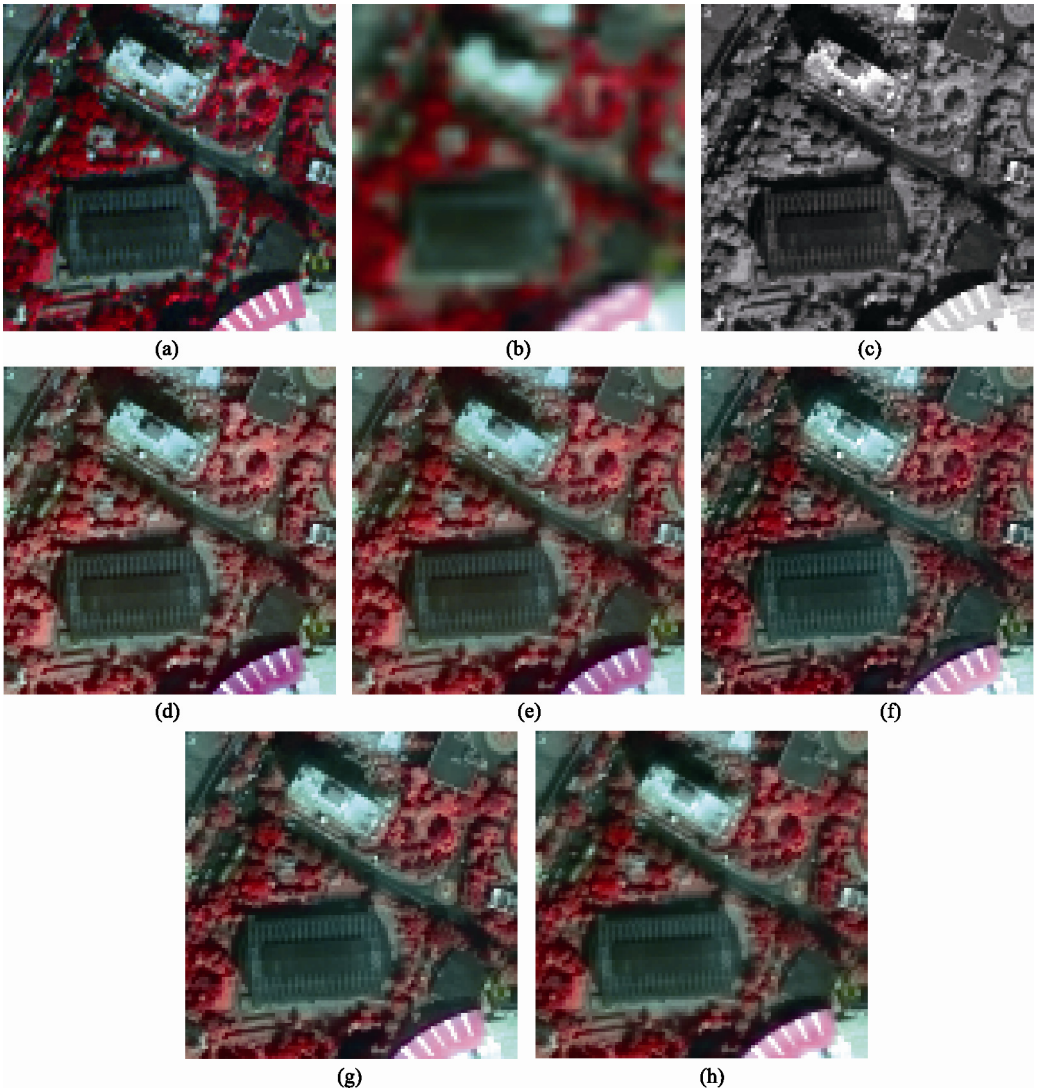

图 3 Quickbird 图像融合结果，所有 MS 图像是 4、3、2 波段的假彩色合成图(为了更好的分析比较，所有显示的图像只是原融合图像的一部分，且进行了放大处理)

(a) 原始 MS 图像; (b) 降质的 MS 图像; (c) 降质的 Pan 图像; (d) GIHS 方法融合的图像; (e) Choi 方法融合的图像; (f) atrWT 方法融合的图像; (g) atrWT+GIHS 方法融合的图像; (h) 新方法融合的图像

为比较各融合算法的性能，采用如下的评价参数:

(1) 光谱相关系数(Correlation coefficient, CC) CC 是指融合图像的各波段和多光谱参考图像对应波段之间相关系数，融合结果光谱信息保持越多，CC 越接近于 1，理想的情况应该是 1;

(2) 相对整体维数综合误差 ERGAS(relative global dimensional synthesis error)(Gonzalez-Audicana, 2004)ERGAS 越低，则融合图像的光谱质量越高，理想情况应该是 0;

(3) 空间相关系数 SCC 本文采用 Zhou 提出的方法 (1998), SCC 越大，表明有越多的空间细节信息“注入”了融合图像。所比较的融合算法主要针对 Tu 的 GIHS 融合方法、Choi 的平衡参数法(Choi, 2006, 平衡参数取 7)、基于 à trous 小波(也称 undecimated wavelet)的融合方法(atrWT)、基于 à trous 小波结合 GIHS 法(atrWT+GIHS)。其中小波变换的实现中，采用双正交紧支撑样条小波(相应于 Matlab 软件中的‘bior2.2’)，分解层数为 3。在算法比较中，采用 à trous 小波主要是考虑到其具有平移不变性，因而图像的融合效果较好。新算法实现中，针对 IKONOS 图像的融合，各个参数设置如下: α=0.01, β=1, γ=0.3, 迭代最大次数 k=16, q=10^{-8}，高斯核为:

$$\boldsymbol{C}=\begin{bmatrix} 0 & -0.25 & 0 \\ -0.25 & 1 & -0.25 \\ 0 & -0.25 & 0 \end{bmatrix}$$

(C)1994-2021 China Academic Journal Electronic Publishing House. All rights reserved. http://www.cnki.net

针对 Quickbird 图像的融合各个参数设置如下: α=0.01, β=1, γ=0.16, 迭代最大次数 k=16, $q=10^{-6}$, 高斯核和 IKONOS 图像实验所采用的相同。

上述各算法的融合图像分别如图 2(d)—(h)、图 3(d)—(h)。实验中算法的融合图像在光谱质量、空间细节质量方面都优于降质的 MS 图像(图 2(b)、图 3(b)), 表明本文算法和其他融合算法都提高融合图像的质量。从光谱质量看, 新算法的融合图像, 其光谱质量和 atrWT 方法、atrWT+GIHS 方法相比难分优劣, 但是略优于 GIHS 方法、Choi 方法。与降质的 MS 图像(图 2(b)、图 3(b))相比, 各融合算法在空间细节上得到很大的提高, 表明 Pan 图像的细节信息被有效地“注入”了 MS 图像, 目视效果上, 图 2(d)—(h)、图 3(d)—(h)在空间细节上区别不明显。

下面从客观评价上对融合图像的光谱质量和空间细节质量进行分析比较:

在表 1、表 2 中, 列出了降质的 MS 图像及上述各种算法的融合图像与参考图像对应波段间的光谱质量参数的数值。

从表 1、表 2 看出, 新算法的 CC 和平均相关系数 $\overline{CC}$ 大于降质图像和参考图像的 CC 及 $\overline{CC}$, 表明新的融合算法提高了光谱质量。新算法的 CC 值在 NIR 波段略低于 atrWT+HIS 方法。而 $\overline{CC}$ 在所有融合算法中最大, ERGAS 值在所有融合算法中最小, 则表明所提的新算法在光谱质量的改善方面优于其他算法。

各融合算法的空间质量比较见表 3、表 4。

由表 3、表 4 可以看出, 几种融合算法经过融合以后的图像, 相比较降质 MS 图像, 在空间细节质量方面都有很大的提高。所提的新融合算法, 其空

表 1 IKONOS 图像融合结果的光谱质量比较

项目		降质	GIHS	Choi	atrWT	atrWT+GIHS	新方法	理想
CC	NIR	0.8703	0.9554	0.9516	0.9598	0.9583	0.9601	1
	R	0.8278	0.9466	0.9475	0.9449	0.9520	0.9557	1
	G	0.8681	0.9589	0.9641	0.9623	0.9659	0.9694	1
	B	0.9361	0.9369	0.9562	0.9558	0.9614	0.9620	1
$\overline{CC}$		0.8756	0.9495	0.9548	0.9557	0.9594	0.9618	0
ERGAS		2.0143	1.3619	1.3595	1.2167	1.1895	1.1607	0

表 2 Quickbird 图像融合结果的光谱质量比较

项目		降质	GIHS	Choi	atrWT	atrWT+GIHS	新方法	理想
CC	NIR	0.8908	0.9369	0.9396	0.9571	0.9699	0.9652	1
	R	0.8925	0.8773	0.9128	0.9357	0.9373	0.9497	1
	G	0.8954	0.8958	0.9288	0.9455	0.9464	0.9587	1
	B	0.9194	0.8836	0.9213	0.9348	0.9361	0.9506	1
$\overline{CC}$		0.8995	0.8984	0.9256	0.9433	0.9474	0.9560	0
ERGAS		1.8836	1.9807	1.7875	1.4456	1.3998	1.2776	0

表 3 IKONOS 图像融合结果的空间质量比较

项目		降质	GIHS	Choi	atrWT	atrWT+IHS	新方法	理想
SCC	NIR	0.7318	0.9860	0.9740	0.9973	0.9873	0.9844	1
	R	0.7323	0.9940	0.9844	0.9920	0.9935	0.9918	1
	G	0.7329	0.9835	0.9694	0.9823	0.9834	0.9806	1
	B	0.7308	0.9867	0.9742	0.9860	0.9868	0.9846	1
$\overline{SCC}$		0.7319	0.9876	0.9755	0.9894	0.9877	0.9853	1

表 4 Quickbird 图像融合结果的空间质量比较

项目		降质	GIHS	Choi	atrWT	atrWT+IHS	新方法	理想
SCC	NIR	0.2385	0.9765	0.9593	0.9932	0.9819	0.9693	1
	R	0.2104	0.9952	0.9892	0.9868	0.9892	0.9859	1
	G	0.2113	0.9939	0.9853	0.9862	0.9885	0.9831	1
	B	0.2017	0.9950	0.9896	0.9872	0.9897	0.9862	1
$\overline{SCC}$		0.2155	0.9902	0.9808	0.9883	0.9873	0.9811	1

(C)1994-2021 China Academic Journal Electronic Publishing House. All rights reserved. http://www.cnki.net

间细节质量优于 Choi 融合算法(平衡参数法), 而和 GIHS 融合算法、atrWT 融合算法、atrWT+IHS 融合算法相当。

考虑到所提的新算法的融合图像光谱质量最好(表 1、表 2), 而 MS 图像与 Pan 图像融合的关键就是在提高融合图像的空间细节质量的同时, 尽可能保持融合图像具有原始 MS 图像的信息, 这表明所提的新算法是可行的。

4 结 论

从新型遥感的光谱特性的物理基础出发, 提出了 GIHS 结合 MAP 框架的新融合方法。新方法主要特点为: 通过 MAP 对 MS 图像的强度分量和 Pan 图像施加一定的限制条件来约束解的范围, 使得融合图像在空间细节质量提高的同时, 较好地保持原始 MS 图像的光谱信息。针对 IKONOS 图像的实验、Quickbird 图像的实验也表明了所提新算法是可行的。融合实现时, 在 MAP 估计的优化迭代过程中, 各个约束参数的选取很关键, 本文是采用试错法来选取。至于如何自适应的选取这些参数, 将是后续的研究工作。

REFERENCES

Choi M. 2006. A new intensity-hue-saturation fusion approach to image fusion with a tradeoff parameter. *IEEE Transactions on Geoscience and Remote Sensing*, **44** (6): 1672—1682

Gonzalez-Audicana M, José L S and Raquel G C. 2004. Fusion of multispectral and panchromatic images using improved IHS and PCA merges based on wavelet decomposition. *IEEE Trasnsactions on Geoscience and Remote Sensing*, **42**(6): 1291—1299

Gonzalez-Audicana M, Otazu X, Fors O and Alvarez-Mozos J. 2006. A low computational-cost method to fuse IKONOS images using the spectral response function of its sensors. *IEEE Transactions on Geoscience and Remote Sensing*, **44**(6): 1683—1691

IKONOS Relative Spectral Response of GeoEye Corporation. 2008. http://www.geoeye.com/CorpSite/resource/white-papers.aspx.

Li X, He M Y, Michel R and Wei B G. 2009. A new algorithm for fusing very high resolution remote sensing images. *Journal of Electronics & Information Technology*, **31**(12): 2886—2891

Mohamed E and Mohammad A. 2008. Superresolution construction of multispectral imagery based on local enhancement. *IEEE Geoscience and Remote Sensing Letters*, **5**(2): 276—279

Pohl C and Van Genderen J L. 1998. Multisensor image fusion in remote sensing: concepts,methods and applications. *International Journal of Remote Sensing*, **19**(5): 823—854

QuickBird Imagery of the Global Land Cover Facility (GLCF) at the University of Maryland. 2005. http://www.landvover.org/data/quickbird

Shah V P, Younan N H and King R L. 2008. An efficient Pan-sharpening method via a combined adaptive PCA approach and Contourlets. *IEEE Transactions on Geoscience and Remote Sensing*, **46**(5): 1323—1335

Song H H, Yu S Y, Song L and Yang X K. 2007. Fusion of multispectral and panchromatic satellite images based on contourlet transform and local averge gradient. *Optical Engineering*, **46** (2): 020502

Thomas C, Ranchin T, Wald L and Chanussot J. 2008. Synthesis of multispectral images to high spatial resolution: a critical review of fusion methods based on remote sensing physics. *IEEE Transactions on Geoscience and Remote Sensing*, **46**(5): 1301—1312

Tu T M, Huang P S, Hung C L and Chang C P. 2004. A fast intensity-hue-saturation fusion technique with spectral adjust- ment for IKONOS imagery. *IEEE Geoscience and Remote Sensing Letters*, **1**(4) : 309—312

Xu J, Guan Z Q, He X F and Hu J W. 2009. Novel method for merging panchromatic and multi-spectral images based on sensor spectral response. *Journal of Remote Sensing*, **13**(1): 97—102

Zhou J, Civco D L and Silander J A. 1998. A wavelet transform method to merge Landsat TM and SPOT panchromatic data. *International Journal of Remote Sensing*, **19**(4):743—757

附中文参考文献

李旭, 何明一, Michel R, 卫宝国. 2009. 一种超高分辨率遥感图像融合新算法. 电子与信息学报, **31**(12): 2886—2891

徐佳, 关泽群, 何秀凤, 胡俊伟. 2009. 基于传感器光谱特性的全色与多光谱图像融合. 遥感学报, **13**(1): 97—102

(C)1994-2021 China Academic Journal Electronic Publishing House. All rights reserved. http://www.cnki.net